Structural, elastic, phonon and electronic properties of a MnPd alloy*

Wang Jun-Fei(王俊斐), Chen Wen-Zhou(陈文周), Jiang Zhen-Yi(姜振益)†,
Zhang Xiao-Dong(张小东), and Si Liang(司 良)

Institute of Modern Physics, Northwest University, Xi'an 710069, *China*

(Received 7 January 2012; revised manuscript received 5 April 2012)

The structural, elastic, phonon and electronic properties of a MnPd alloy have been investigated using the first-principles calculation. The calculated lattice constants and electronic structure agree well with the experimental results. The microscopic mechanism of the diffusionless martensitic transition from the paramagnetic B2 (PM-B2) phase to the antiferromagnetic $L1_0$ (AFM-$L1_0$) phase through the intermediate paramagnetic $L1_0$ (PM-$L1_0$) phase has been explored theoretically. The obtained negative shear modulus $C' = (C_{11} - C_{12})/2$ of the PM-B2 phase is closely related to the instability of the cubic B2 phase with respect to the tetragonal distortions. The calculated phonon dispersions for the PM-$L1_0$ and AFM-$L1_0$ phases indicate that they are dynamically stable. However, the AFM-$L1_0$ phase is energetically most favorable according to the calculated total energy order, so the PM-$L1_0$ →AFM-$L1_0$ transition is caused by the magnetism rather than the electron–phonon interaction. Additionally, the AFM-$L1_0$ state is stabilized through the formation of a pseudo gap located at the Fermi level. The calculated results show that the CuAu-I type structure in the collinear antiferromagnetic state is dynamically and mechanically stable, thus is the low temperature phase.

Keywords: transition metals and alloys, density functional theory, band structure, elasticity

PACS: 71.20.Be, 1.15.Mb, 1.20.–b, 2.20.D– **DOI:** 10.1088/1674-1056/21/7/077102

1. Introduction

It is known that the $L1_0$-type ordered equiatomic MnM (M =Ni, Pd, Pt, Rh, and Ir) alloy systems show high stability with very high Néel temperatures. Due to excellent properties such as large exchange coupling fields and high blocking temperatures deeply related to the high antiferromagnetic stability,[1−3] they have been intensively investigated for practical applications such as spin-valve layers for giant magnetoresistance (GMR)[4−7] and tunneling magnetoresistance (TMR) device heads.[8−13] The high blocking properties of the above alloys originates from the martensitic twin formed through the martensitic transition (fcc→fct). Hence, it is necessary to study the microscopic mechanism of the martensitic transition to develop superior magnetic materials. However, up to now, little theoretical research has been done about the martensitic transition for the $L1_0$–type equiatomic MnM (M=Ni, Pd, Pt, Rh, and Ir) alloys.

At high temperatures, the equiatomic MnPd alloy forms a B2 (CsCl)-type paramagnetic cubic structure, and transforms into the $L1_0$ (CuAu-I)-type collinear antiferromagnetic tetragonal structure at low temperatures with a diffusionless martensitic process.[14] According to the experimental measurements of magnetic susceptibility and electrical resistivity of MnPd,[15−17] above 920 K, the equiatomic MnPd crystal structure is the B2 (CsCl)-type ($Pm3m$) ordered paramagnetic cubic structure, at 920 K, the B2 structure transforms to a paramagnetic tetragonal structure called the $L1_0$ (CuAu-I)-type ordered structure. When the annealing temperature further decreases, the antiferromagnetic transition occurs around 780 K. The phase transition can be validly revealed by means of lattice dynamic instabilities, and the phonon dispersion relations can examine local as well as global stability and investigate the mechanisms of the martensitic transitions. Meanwhile, the phase stability and the transition behavior are closely related to their electronic structures and elastic properties. However, the theoretical and experimental studies of phonon dispersion and elastic properties of MnPd have not been reported yet. Therefore, in this work, we investigate

*Project supported by the National Natural Science Foundation of China (Grant Nos. 10647008 and 50971099) and the Research Fund for the Doctoral Program of Higher Education, China (Grant No. 20096101110017).

†Corresponding author. E-mail: jiangzy@nwu.edu.cn

the structural, elastic, phonon, and electronic properties of MnPd by using *ab intio* density functional calculations. According to the calculated results, the microscopic mechanism of the martensitic transition of the equiatomic MnPd alloy is interpreted well. The rest of this paper is organized as follows. The method of calculation is given in Section 2, the results are discussed in Section 3. Finally, a general conclusion is given in Section 4.

2. Theoretical method

All density functional calculations were performed using the Vienna *ab initio* simulation package (Vasp-MedeA package)[18,19] with projector augmented-wave (PAW) potentials,[20,21] the generalized gradient approximation (GGA), and the exchange–correlation functional of Perdew *et al.*[22] (denoted as PBE hereafter). An energy cut-off of 450 eV was found to be adequate for the calculation of the structural, elastic, phonon and electronic properties. The pseudopotentials represented $3p^6 4s^1 3d^6$ and $4p^6 5s^1 4d^9$ electron configurations for Mn and Pd, respectively. A $17 \times 17 \times 17$ Monkhorst–Pack[23] grid of k-points was used for the integration in the irreducible Brillouin zone for all phases. The relaxation of geometry optimization was performed until the total energy change was within the 10^{-6} eV per atom, the Hellmann–Feynman forces on all atomic sites were computed for positive and negative displacements with the amplitude of 0.02 Å. Our calculation of phonon dispersion relations for PM-$L1_0$ and AFM-$L1_0$ structures were conducted with MedeA-Phonon in conjunction with MedeA-Vasp by using the direct method.[24] The lattice-dynamics calculation was carried out with a larger supercell. We used a $2 \times 2 \times 3$ supercell containing 48 atoms, and the requested k-spacing of 0.5/Å led to a $2 \times 2 \times 2$ q-mesh. All calculations for the PM-B2 and PM-$L1_0$ structures were performed without spin polarization. The spin polarization calculation was necessary for the AFM-$L1_0$ structure.

3. Results and discussion

3.1. Structure properties

We adopt experimental lattice constants to initialize the geometrical optimization. The calculated and the previous theoretical and experimental results of the space group, lattice constants, volume, energy difference ΔE from the minimum energy for AFM-$L1_0$ and the local moment m_{Mn} for AFM-$L1_0$ are summarized in Table 1. The optimized crystal structure of PM-B2 is the CsCl-type ($Pm3m$) cubic structure with the Mn and Pd atoms respectively occupying the corners and the center of the cube with a lattice constant of 2.998 Å, which is a little smaller than the observed value of 3.15 Å[16] with an error of 4.8%. The experimental magnetic structure of AFM-$L1_0$ MnPd is shown in Fig. 1,[15] where the Mn moments are coupled antiferromagnetically in the c-plane, and the moments between the nearest neighbor layers of Mn atoms are coupled ferromagnetically. It has been found that the AFM-$L1_0$ phase is the ground state with $a = 3.992$ Å and $c = 3.694$ Å ($c/a = 0.925$), which are very close to the observed values of $a = 4.072$ Å and $c = 3.58$ Å ($c/a = 0.88$)[15] and also to the calculated ones by Yamada *et al.*[25] The calculated AFM-$L1_0$ structure with the minimum energy has $P4/mmm$ space group with atomic positions of Mn (0, 0, 0), Mn (1/2, 1/2, 0), Pd (1/2, 0, 1/2), and Pd (0, 1/2, 1/2). The local magnetic moment is 3.78 μ_{B} on the Mn site, which is smaller than the experimental value of about 4.4 μ_{B}[15] and close to the previously calculated 3.8 μ_{B}.[21] The Pd sublattice moment is found to be zero. Because of a lack of experimental lattice constants for the intermediate

Table 1. Calculated space group (SG), equilibrium lattice constants a and b, volume V, magnetic moment m_{Mn}, and energy difference ΔE from the minimum energy for AFM-$L1_0$.

Structure	SG	a/ Å	c/ Å	V/Å^3	$m_{\mathrm{Mn}}/\mu_{\mathrm{B}}$	ΔE/eV·atom^{-1}
PM-B2	$Pm3m$	2.998	2.998	26.946	0	0.865
PM-B2[a)]	$Pm3m$	3.15	3.15	31.256	0	–
PM-$L1_0$	$P4/mmm$	2.630	3.807	26.333	0	0.617
PM-$L1_0$[b)]	$P4/mmm$	2.60	3.90	26.364	0	–
AFM-$L1_0$	$P4/mmm$	3.992	3.694	58.868	3.78	0.00
AFM-$L1_0$[c)]	$P4/mmm$	4.072	3.580	59.361	4.4	–
AFM-$L1_0$[d)]	$P4/mmm$	4.086	3.6	60.103	4.08	–

[a)]Experimental results form Ref. [16]; [b)d)]calculated results from Ref. [25];[c)]experimental results from Ref. [15].

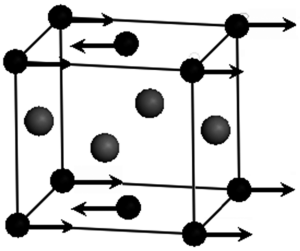

Fig. 1. Crystal structure with spin structure for $L1_0$-type MnPd ordered alloy in the AFM state. The Mn and Pd sites are marked by black and gray balls, respectively.

PM-$L1_0$ structure, we determine its equilibrium lattice parameters by optimizing the previous experimental lattice constants of AFM-$L1_0$ mainly for comparing the total energies for the three states. The optimized lattice parameters for PM-$L1_0$ are determined to be of the $P4/mmm$ space group with Wyckoff sites of Mn (0.0, 0.0, 0.0) and Pd (1/2, 1/2, 1/2), and its volume is smaller than that of the calculated AFM-$L1_0$ with an error of 10.53%. The total energies for all phases are obtained by relaxing all structural constants, angles, and internal atomic coordinates with equal convergence standards. The calculated total-energy order PM-B2 > PM-$L1_0$ > AFM-$L1_0$ means that the PM-B2 structure first relaxes to the tetragonal phase without local moments on all atoms, and then to the collinear antiferromagnetic tetragonal phase spin ordering, which is in accordance with the experimental results.[17] In addition, it is well known that the volume conserving martensitic transition is a necessary and sufficient condition for shape memory alloy effect in systems with a cubic austenitic phase. However, a major volume expansion of the 1.244 Å^3 per atom exists for the transition from the PM-B2 structure to the AFM-$L1_0$ structure according to Table 1, which shows that the stoichiometry MnPd alloy does not have a shape memory behavior. Furthermore, we employ the above obtained crystal parameters of the PM-B2 and the AFM-$L1_0$ phases to analyse their mechanical stabilities by calculating their elastic constants.

3.2. Elastic constants and phonon dispersion

The elastic constants can provide a link between the mechanical and dynamic behavior of the crystals. They also give important information concerning the nature of the forces operating in the solids and provide information on the stability and the stiffness of the materials, especially for the martensitic transition. Expanding the total energy in a Taylor series can provide the elastic constants C_{ij}. To the second order, the total energy is expressed as

$$E(V, e_i) = E(V_0, 0) + V_0 \sum_{i=1}^{6} \sigma_i e_i + \frac{V_0}{2} \sum_{i,j=1}^{6} C_{ij} e_i e_j + \cdots , \quad (1)$$

where V_0 is the volume of the unstrained crystal, and $E(V_0,0)$ is the corresponding energy. To study the relationship between the transition behavior and the elastic properties, all elastic constants for the PM-B2 and AFM-$L1_0$ phases are calculated and shown in Table 2. To the best of our knowledge, comparative experimental and the other theoretical data have not been obtained. The number of independent elastic constants is different for structures with different symmetries. There are 3 independent elastic constants (C_{11}, C_{12}, and C_{44}) for the cubic structure and 6 (C_{11}, C_{12}, C_{13}, C_{33}, C_{44}, and C_{66}) for the tetragonal structure. For a cubic lattice, the basal plane shear modulus $C' = (C_{11} - C_{12})/2$ is related to the elastic constant softening, which is a common feature both in temperature-induced and stress-induced martensitic transitions. In view of its importance, we obtain the C'. The criteria for mechanical stability[26,27] are presented as $C_{11} > 0$, $C_{44} > 0$, $C_{11} + 2C_{12} > 0$, and $C_{11} - C_{12} > 0$. For a tetragonal crystal, the conditions of $C_{11} > 0$, $C_{33} > 0$, $C_{44} > 0$, $C_{66} > 0$, $C_{11} - C_{12} > 0$, $C_{11} + C_{33} - 2C_{13} > 0$, and $2C_{11} + C_{33} + 2C_{12} + 4C_{13} > 0$ must be satisfied when the tetragonal crystal is mechanically stable.[28,29] For the PM-B2 cubic phase, when B, C', and C_{44} are positive, it is mechanically stable. All our calculated elastic constants obey the mechanical stability criteria except for C'. The calculated negative C' indicates the instability of the PM-B2 cubic phase with respect to the tetragonal distortions, which is in accordance with the experimental results.[17] Only C_{44} has a non-negative value at 0 K. Therefore, C' should go to zero at the transition temperature of the cubic to tetragonal phase, while C_{44} should still be positive. On the other hand, our calculated results for the elastic constants of the PM-$L1_0$ and AFM-$L1_0$ structures listed in Table 2 satisfy the stability conditions, implying their nice mechanical stability. It is also well known that the shear modulus C' characterizes the stability of the lattice under the shear deformation and is related to the tetragonal distortions. Thus, our calculations suggest that the softening of C' to zero triggers the cubic to the tetragonal phase transition path.

Table 2. Calculated elastic constants (in the units of GPa) of PM-B2 and AFM-$L1_0$ MnPd structures.

Structure	C_{11}	C_{12}	C_{13}	C_{33}	C_{44}	C_{66}	C'
PM-B2	105.7	251.8	–	–	128.4	–	−73.1
PM-$L1_0$	391.5	110.1	162.8	326.3	152.4	73.2	140.7
AFM-$L1_0$	204.7	85.4	118.5	220.8	104.9	91.2	59.7

In order to further check the dynamical stability of the PM-$L1_0$ and AFM-$L1_0$ phases, the dynamical phonon dispersions are computed. The phonon dispersions play an important role in understanding the physical properties of solid materials, including the specific heat, thermal expansion, heat conduction and electron–phonon coupling. The obtained phonon spectrum shape of the PM-$L1_0$ structure is nearly the same as that of the AFM-$L1_0$ structure, so we only draw the phonon spectrum for the AFM-$L1_0$ structure. The calculated phonon spectra along the high-symmetry directions Γ–Z throughout the Brillouin zone for the AFM-$L1_0$ phase are illustrated in Fig. 2. The *ab initio* force constant direct approach described in the computational method section is used. It is clearly seen that a very small imaginary frequency exists at the Γ point in the reciprocal space. This imaginary frequency is generated because of the anharmonic approximation and does not bring out any atomic shift. Therefore, not surprisingly, the calculated phonon spectra do not contain soft modes at any direction (expect for the Γ point), which confirms that the AFM-$L1_0$ phase is dynamically stable. Similarly, we can confirm that the PM-$L1_0$ structure also has dynamical stability at low temperature. Hence, different from the reason for the martensitic transition,[30] the antiferromagnetic transition from the PM-$L1_0$ to AFM-$L1_0$ structure is not reduced by the electron–phonon interaction but by the magnetism.

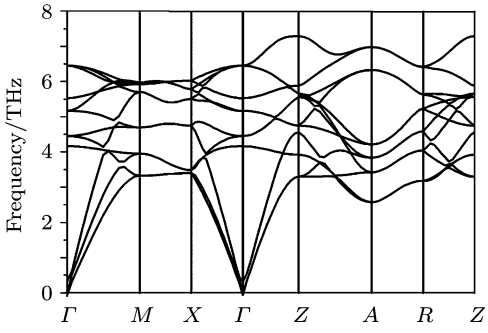

Fig. 2. Phonon dispersion relation for the MnPd alloy in the $L1_0$ collinear antiferromagnetism state.

3.3. Electronic properties

In consideration of the relation between the features of electronic density of state (DOS) at the Fermi level (E_F) and the phase transition, the total DOS at E_F is an important indication of the stability of alloys.[31] We show the results of calculations for the total DOS (ranging from about –8 eV to 4 eV) for the PM-B2 and AFM-$L1_0$ states with the calculated equilibrium lattice constants in Figs. 3 and 4 respectively to explore the underlying transition mechanism. Generally speaking, the higher stability corresponds to a lower total DOS at E_F. For PM-B2, the E_F lies in the higher energy peaks of the DOS, and the value of the total DOS at E_F is about 6.3 state/eV per unit cell in Fig. 3. It is seen that the PM-B2 structure has a relatively higher electronic DOS at E_F. However,

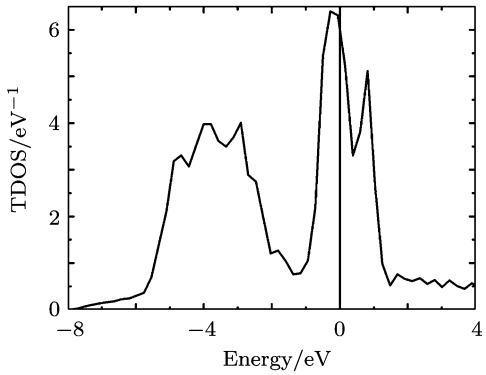

Fig. 3. Total density of state of a MnPd alloy in the B2 paramagnetic state.

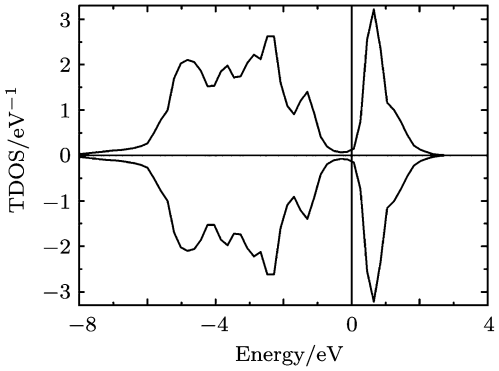

Fig. 4. Total density of state of a MnPd alloy in the $L1_0$ collinear antiferromagnetism state.

the situation changes dramatically around the $E_{\rm F}$ for the AFM-L1$_0$ state with a very small but finite intensity at $E_{\rm F}$ in Fig. 4, which is caused by the formation of a pseudo gap. The formation of the characteristic pseudo gap around the Fermi level is attributed to the antiferromagnetic staggered field caused by the antiferromagnetic spin arrangement. In addition, the DOS at $E_{\rm F}$ of AFM-L1$_0$, which is very small (about 0.2 state/eV per unit cell, regarding 0.5 unit cell of AFM-L1$_0$ as the unit cell), and the rather clear dip structure around the $E_{\rm F}$ are in agreement with the small theoretical and experimental values of the electronic specific heat coefficient as well as the temperature dependence of electrical resistivity (ρ–T) measured in Refs. [17] and [32]. It is obvious that the total DOS for AFM-L1$_0$ is much smaller than that for PM-B2 at the E_F, indicating that AFM-L1$_0$ is more stable than the PM-B2 cubic structure at low temperature in accordance with the experimental results.[15−17]

4. Conclusion

In conclusion, we seek to understand why the martensitic transition of PM-B2→AFM-L1$_0$ occurs during annealing at the atomic level. The structural, elastic, phonon and electronic properties of the PM-B2, PM-L1$_0$, and AFM-L1$_0$ phases are taken into account based on the density-functional theory within the generalized gradient approximation (GGA). The calculated lattice parameters are reasonable with the available experimental data and the other theoretical results. Total energies and total DOS calculations indicate that the AFM-L1$_0$ phase is energetically more favorable. By analyzing the elastic constants, the negative shear modulus $C' = (C_{11} - C_{12})/2$ of the PM-B2 phase is closely related to the instability of the PM-B2 cubic phase with respect to the tetragonal distortions. The calculated elastic constants and phonon spectra for PM-L1$_0$ and AFM-L1$_0$ structures confirm their dynamical and mechanical stability, which indicates that the magnetism leads to the antiferromagnetic transition (PM-L1$_0$ →AFM-L1$_0$). The characteristic pseudo gap around the $E_{\rm F}$ of DOS for the AFM-L1$_0$ structure demonstrates its antiferromagnetic structure, and is consistent with the available experimental data and the other theoretical calculations. All the above calculated results confirm the martensitic transition path from the PM-B2 phase to the AFM-L1$_0$ phase proceeding through the intermediate PM-L1$_0$ phase at the atomic level.

References

[1] Lin T, Gorman G L and Tsang C 1996 *IEEE Trans. Magn.* **32** 3443

[2] Farrow R F C, Marks R F, Gider S, Marley A C, Parkin S S P and Mauri D 1997 *J. Appl. Phys.* **81** 4986

[3] Kishi H, Kitade Y, Miyake Y, Tanaka A and Kobayashi K 1996 *IEEE Trans. Magn.* **32** 3380

[4] Prakash S, Pentek K and Zhang Y 2001 *IEEE Trans. Magn.* **37** 1123

[5] Saito M, Hasegawa N, Koike F, Seki H and Kuriyama T 1999 *J. Appl. Phys.* **85** 4928

[6] Khapikov A, Simion B and Lederman M 2003 *J. Appl. Phys.* **93** 7313

[7] Morales E H, Wang Y, Lederman D, Kellock A J and Carey M J 2003 *J. Appl. Phys.* **93** 4729

[8] Schwickert M M, Childress J R, Fontana R E, Kellock A J, Rice P M, Ho M K, Thompson T J and Gurney B A 2001 *J. Appl. Phys.* **89** 6871

[9] Childress J R, Schwickert M M, Fontana R E, Ho M K, Rice P M and Gurney B A 2001 *J. Appl. Phys.* **89** 7353

[10] Zhou G H, Wang Y G, Qi X J, Li Z Q and Chen J K 2009 *Chin. Phys.* B **18** 790

[11] Qi X J, Wang Y G, Zhou G H, Li Z Q and Guo M 2010 *Chin. Phys.* B **19** 037503

[12] Qi X J, Wang Y G, Miao X F, Li Z Q and Huang Y Z 2010 *Chin. Phys.* B **19** 037505

[13] Qi X J, Wang Y G, Miao X F, Li Z Q and Huang Y Z 2011 *Chin. Phys.* B **20** 057503

[14] Raub E and Mahler W 1955 *Z. Metallkd.* **46** 282

[15] Pál L, Krén F, Kádár G, Szabó P and Tarnóczi T 1968 *J. Appl. Phys.* **39** 538

[16] Raub E and Mahler W 1954 *Z. Metallkd.* **45** 430

[17] Umetsu R Y, Fukamichi K and Sakuma A 2002 *J. Magn. Magn. Mater.* **239** 530

[18] Kresse G and Hafner J 1993 *Phys. Rev.* B **47** 558

[19] Kresse G and Furthmuller J 1993 *Phys. Rev.* B **54** 11169

[20] Blöchl P E 1994 *Phys. Rev.* B **50** 17953

[21] Kresse G and Joubert D 1999 *Phys. Rev.* B **59** 1758

[22] Perdew J P, Burke K and Ernzerhof M 1996 *Phys. Rev. Lett.* **77** 3865

[23] Monkhorst H J and Pack J D 1976 *Phys. Rev.* B **13** 5188

[24] Parlinski K, Li Z Q and Kawazoe Y 1997 *Phys. Rev. Lett.* **78** 4063

[25] Yamada W, Shimizu H, Yamamoto K and Uebayashi K 2006 *J. Alloys Compounds* **415** 31

[26] Wang J, Yip S, Phillpot S R and Wolf D 1993 *Phys. Rev. Lett.* **71** 4182

[27] Shpakov V P, Tse J S, Belosludov V R and Belosludov R V 1997 *J. Phys.*: *Condens. Matter* **9** 5853

[28] Beckstein Q, Klepeis J E, Hart G L W and Pankratov O 2001 *Phys. Rev.* B **63** 134112

[29] Chen X, Fu C L and Morris J R 2010 *Intermetallics* **18** 998

[30] Chen W Z, Jiang Z Y, Si L, Li L S and Zhou B 2011 *Solid State Commun.* **151** 1433

[31] Ye Y Y, Chan C T and Ho K M 1997 *Phys. Rev.* B **56** 3678

[32] Umetsu R Y, Fukamichi K and Sakuma A 2006 *J. Phys. Soc. Jpn.* **75** 104714